Journal of University of Duhok, Vol. 20, No.1 (Pure and Eng. Sciences), Pp 285-292, 2017
eISSN: 2521-4861 & pISSN: 1812-7568
https://doi.org/10.26682/sjuod.2017.20.1.26

# THE EFFECT OF SOIL WATER RETENTION CURVE HYSTERESIS ON THE STRENGTH OF UNSATURATED SOILS.

**B**ESTUN **S**HWAN
Dept. of Geotechnical Engineering, College of Engineering, University of Koya, Kurdistan Region-Iraq

## ABSTRACT

**A modification of an existing soil water retention curve (SWRC) equation is presented in this paper which takes into consideration the effects of the soil capillarity (parameter *a*) and air entry value ($s_o$). The reformulated equation then was incorporated into the research version of the LimitState:GEO software to perform two parametric studies on the bearing capacity of a strip footing placed on the surface and total passive earth pressure for a frictional wall of 1 m height. The parametric analyses were to study the effect of SWRC hysteresis on the strength of unsaturated soils through parameter *a* and air entry value ($s_o$). The numerical bearing capacity and the passive earth pressure results were compared with the experimental data and the derived Rankine equations which take into account the effect of capillary rise, respectively. The numerical results showed that the effect of SWRC hysteresis has significant influence on the strength for both parametric studies.**

***KEYWORDS:*** SWRC, Evaluation, Modification, Unsaturated Soil.

## 1. INTRODUCTION

The relationship between soil suction and volumetric water content is widely used in unsaturated soil mechanics and it is called soil water retention curve (SWRC). The volumetric water content is often replaced by gravimetric water content or degree of saturation. The SWRC is usually determined from laboratory tests by applying a constant or null level of net stress.

Figure 1 shows a typical SWRC illustrating some useful features and capillary hysteresis. Air entry value is the matric suction where air starts to enter the largest pores in the soil, while residual suction is the suction where a large change in suction is required to remove additional water from the soil, Fredlund & Xing (1994).

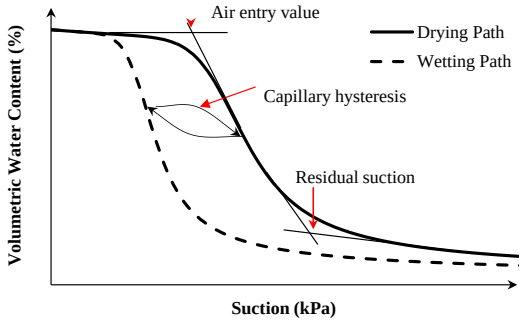


**Fig. (1):** Typical soil water retention curve (SWRC) showing capillary hysteresis.

The importance of studying the SWRC is attributed to that it can be used to estimate several parameters in the field of unsaturated soil mechanics such as permeability and shear strength, Fredlund & Rahardjo (1993). Several mathematical equations, therefore, have been proposed to simulate the SWRC.

Brooks & Corey (1964) suggested an empirical equation for the SWRC which is a relationship between normalized water content ($\theta$) and suction ($s$). The equation took into consideration air entry value ($s_a$) of the soil.

$$\theta = \left[\frac{s_a}{s}\right]^{\beta} \quad (1)$$

where $\beta$ is pore size distribution index. Equation 1 simulated the experimental data for a range of suctions greater than air entry value. However, it is not suitable for any suction value less than air entry value near the saturation.

Van Genuchten (1980), then, proposed another equation for the SWRC to fully define the shape of the SWRC and for any value of suction with more number of parameters.

$$\theta = \left[\frac{1}{1+(\alpha\, s)^{n}}\right]^{m} \quad (2)$$

Journal of University of Duhok, Vol. 20, No.1 (Pure and Eng. Sciences), Pp 285-292, 2017
eISSN: 2521-4861 & pISSN: 1812-7568
https://doi.org/10.26682/sjuod.2017.20.1.26

where $\alpha$, $n$ and $m$ are fitting parameters. It is obvious that Eq. 2 has two more parameters than Eq. 1 which provides better fitting of data and flexibility to simulate the shape of the SWRC. Van Genuchten (1980) utlised Eq. 2 to estimate hydraulic conductivity of the soil by suggesting $m = 1- (1/n)$. Fredlund & Xing (1994) criticized that better fitting can be obtained without using a fixed relationship of $m$.

Fredlund & Xing (1994) also suggested an SWRC equation as follows:

$$\theta = C(s)\,\theta_s \left[ \frac{1}{\ln(e + (\frac{s}{a})^n} \right]^m \quad (3)$$

$$C(s) = \theta_s \left[ 1 - \frac{\ln[1 + (\frac{s}{s_r})]}{\ln[1 + (\frac{10^6}{s_r})]} \right]^m \quad (4)$$

where $\theta_s$ is saturated volumetric water content, $e$ = 2.718, $s$ is suction, $a$, $n$ and $m$ are fitting parameters, $C(s)$ is a correction factor and $s_r$ is residual suction.

Fredlund & Xing (1994) equation requires 4 parameters. Although the fitting parameters can be assumed for the best fitting, what it can be seen is that the integration of Eqs. 2 and 3 is difficult because of high number of the fitting parameters.

Finally, Stanier & Tarantino (2010) suggested an exponential equation for the SWRC as:

$$S_r = e^{-a\,s} \quad (5)$$

where $a$ is a fitting parameter ($kPa^{-1}$), $s$ is hydrostatic suction and it is given by:

$$s = \gamma_w (H_w - z) \quad (6)$$

where $\gamma_w$ is unit weight of water ($kN/m^3$), $H_w$ is water table depth (positive downward) and $z$ is vertical coordinate (positive downward). Equation 5 shows a simple mathematical relationship between degree of saturation and suction with only one fitting parameter ($a$) and assumes full water continuity within the soil. It is obvious from Fig. 1 that the shape of the SWRC follows an exponential function within a range of suction values between air entry value and residual suction. However, Eq. 5 cannot fit the full shape of the SWRC.

This paper is, therefore, presents a modification of the existing SWRC equation (Eq. 5). The modified equation takes into consideration the effects of the capillary rise and air entry value (SWRC hysteresis). The reformulated equation is, then, incorporated into a research version of the LimitState:GEO software where parametric studies on bearing capacity and earth pressures are conducted.

## 2. MODIFICATION OF THE SWRC EQUATION

Shwan and Smith (2014) reformulated Eq. 5 for more flexible fitting the shape of the SWRC as follows:

$$S_r = 1 \quad (7)$$

$$S_r = e^{-a\,(s - s_o)} \quad (8)$$

where $s_o$ is air entry value (kPa) and it is related to capillary rise, $H_c$ (full saturation) of the soil as:

$$H_C = H_W + \frac{s_o}{\gamma_W} \quad (9)$$

Similarly to Eq. 5, Eqs. 7 and 8 display the simplicity. Also, the most important advantages of Eqs. 7 and 8 over Eq. 5 is that Eq. 8 takes into account the effect of the air entry value. It is intriguing that Eq. 8 only requires two parameters $a$ and $s_o$, while Eqs. 2 and 3 require three and four parameters, respectively.

The linking between the SWRC and shear strength is essential. Vanapalli (1996) proposed a direct relationship between the SWRC of soils and the shear strength through which the shear strength can be estimated. The effect of degree of saturation, which can be obtained directly from the SWRC neglecting drying and wetting of the SWRC, on shear strength of unsaturated soils is significant. Shear strength equations for unsaturated soils have been proposed with a direct relationship between suction and degree of saturation. Among the most widely used equations is the one proposed by Öberg & Sällfors (1997).

$$\tau = c' + (\sigma + sS_r)\tan\phi' \quad (10)$$

where $\tau$ is the shear strength (kPa), $c'$ is the effective cohesion (kPa), $\sigma$ is the normal stress (kPa) and $\phi'$ is the effective internal friction angle.

The term $sS_r \tan\phi'$ represents the effect of water pressure (suction) while also allowing for

Journal of University of Duhok, Vol. 20, No.1 (Pure and Eng. Sciences), Pp 285-292, 2017
eISSN: 2521-4861 & pISSN: 1812-7568
https://doi.org/10.26682/sjuod.2017.20.1.26

the reduced effective area of action due to the reduction of water content. The term also characterises the effect of an increase in strength that can be earn due to unsaturated conditions. For the computational analyses, Eqs. 2 or 3 can be substituted into Eq. 10 to predict shear strength of unsaturated soils. However, integration of Eqs. 2 or 3 is difficult due to the high numbers of the parameters used.

## 3. INTEGRATION OF THE MODIFIED SWRC EQUATIONS

The stability of the soil is significantly influenced by the shear forces along a failure line (discontinuity). The increase of shear strength for unsaturated conditions is attributed to development of apparent cohesion forces along any failure/or slip lines. This increase will be termed "apparent cohesion" through the manuscript of this paper. To derive the apparent cohesion forces along the slip line, Fig. 2 presents a body of soil above a discontinuity showing the shear force (F) and strip weight (W) above the discontinuity.

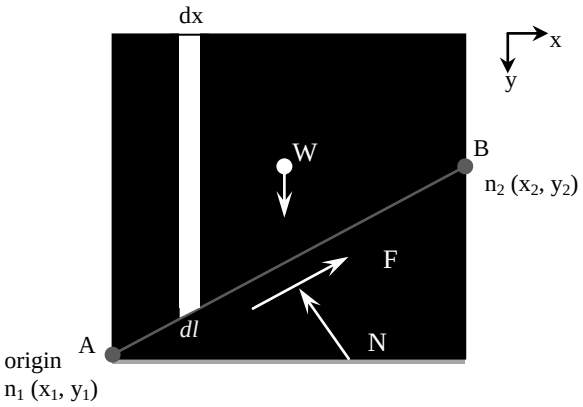


**Fig. (2):** A block of soil above a discontinuity.

Integration of the yield equation for a partially saturated soil along the discontinuity AB can be obtained using the following:

$$A' = \int_{o}^{L} sS_r \tan\phi'.dl \qquad (11)$$

where $A'$ is apparent cohesion force and $L$ is length of the discontinuity AB. By substituting Eqs. 7 or 8 into Eq. 11, apparent cohesion force can be easily computed at different saturation conditions. However, the integration might not be straightforward when using Eqs. 2 or 3 due to the difficulties associated to the high number of parameters utilised in the equations.

Figure 3 shows a retaining wall case study for a discontinuity crossing the water table. The effect of degree of saturation can be easily studied through derivation of the apparent cohesion forces along the failure line.

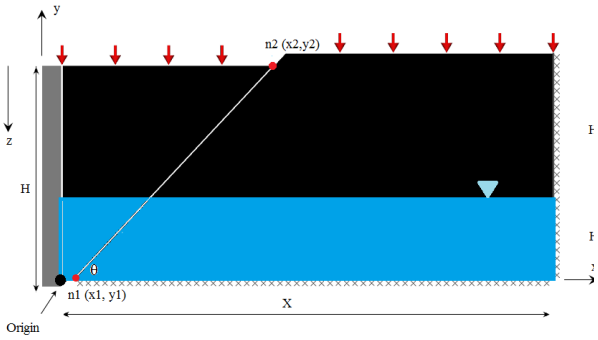


**Fig. (3):** A retaining wall case study with a slip line.

For the origin shown in Fig. 3, Eq. 6 requires redefining in an (x, y) coordinate system so that (y) can measured positive upward from the base of the wall, while $H_1$ is the height of the water table from the origin and it given as:

$$z = H - y = H_1 - H_2 - y \qquad (12)$$

By rearranging Eq. 12, the following can be obtained:

$$z - H_2 = H_1 - y \qquad (13)$$

where $H$, $y$, $H_1$ and $H_2$ are defined in Fig. 3. By substituting Eq. 13 into Eq. 6, the following can be obtained:

$$s = \gamma_w (y - H_1) \qquad (14)$$

where $y = y_1 + l \sin\phi$ based on Fig. 2. Then, by substituting Eqs. 8 and 14 into Eq. 11, the apparent cohesion force for the case shown in Fig. 3 (for a discontinuity crosses the water table) can be computed easily. The integration consists of two parts, part below the water table and part above the water table as follows:

$$A' = \int_{0}^{L_1} s \tan\phi'.dl + \int_{0}^{L_2} sS_r \tan\phi'.dl \qquad (15)$$

For the first part of the integration, $S_r$ = 1. where $L_1$ and $L_2$ are length of the discontinuity below and above the water table, respectively. By substituting Eqs. 8 and 14 into Eq. 15, integrating

Journal of University of Duhok, Vol. 20, No.1 (Pure and Eng. Sciences), Pp 285-292, 2017
eISSN: 2521-4861 & pISSN: 1812-7568
https://doi.org/10.26682/sjuod.2017.20.1.26

and substituting the boundary conditions the following can be obtained:

$$A' = \gamma_w \tan\phi' \left[ \begin{array}{l} \frac{H_1^2}{2}\sin\phi' + H_1(y_1 - H_1) - \\ (a\gamma_w \sin\phi' L_2 + 1)\left(\frac{e^{-a\gamma_w L_2 \sin\phi' + a\, s_o}}{(a\gamma_w)^2 \sin\phi'}\right) \end{array} \right] \quad (16)$$

Similarly to above, integration of other cases when the discontinuity is totally above or below the water table can be derived readily and is not presented in this paper.

#### 4. EFFECT OF PARAMETER "*a*" ON THE SWRC

Figure 4 shows SWRCs for various values of parameter *a* in which different curves are introduced. These variations of *Sr* at the same *s* for different *a* values can be used to represent different soil types at the same air entry value (i.e. 5 kPa). This has advantage of varying capillary range of the soil in which significant increase in *Sr* can be seen for two different *a* values at same suction. Expanding capillary range of soil by parameter *a* can be represented particle size of the soil. Therefore; with parameter *a*, different soil types (even at the same air entry value) can be modelled and this is provides flexibility of the used equation (Eq. 8) for representing the SWRC. The proposed Eq. 8 is a simplified equation when it is compared to the Van Genuchten (1980) or Fredlund and Xing (1994) with less numbers of fitting parameters.

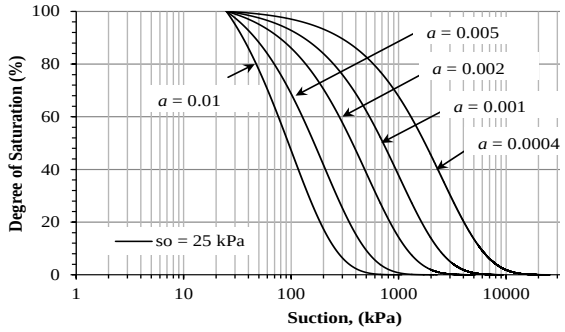


**Fig. (4):** Various SWRCs at $s_o$ = 25 kPa at different values of parameter *a*.

## 5. EFFECT OF AIR ENTRY VALUE " $s_o$ " ON THE SWRC

Figure 5 presents an example of the effect of the air entry value ($s_o$) on the SWRC which is obtained using Eq. 8. The curves represent various values for $s_o$ at the same $a$ = 0.002. Once again, different $s_o$ represents different soil types. The higher the $s_o$ value, the steeper curve can be produced.

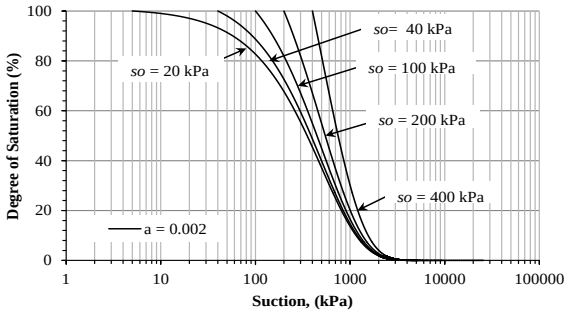


**Fig. (5):** Various SWRCs for $a$ = 0.002 at different values of air entry value ($s_o$).

## 6. CASE STUDIES

### (a) bearing capacity results:

A parametric study using a strip footing of a width of 0.025m was modelled using the LimitState:GEO software, modified by Shwan (2015) to take into account the effect of suction and degree of saturation on strength. The x and y boundaries of the problem were 0.6 and 0.1m, respectively. Soil was assumed to be fully saturated below the capillary rise and an average between dry and saturated unit weights were taken for the zone above the capillary rise.

The numerical results were compared with experimental data conducted by Shwan (2015) using a fine sand. The physical and shear strength parameters of the sand tests are shown in Table 1. The SWRC for the sand tested was determined by means of the hanging column technique and filter paper method, see Shwan (2016). The unsaturated soil parameters $a$ and $s_o$ were 0.7 and 2.3 kPa, respectively. The applied suction used in this parametric study was 5.58 kPa (head of 0.568 m from the soil surface to the water table). This value of suction corresponded to an average degree of saturation of 10% (based on the SWRC).

Table 1 Physical and shear strength properties of the sand used.

| $\gamma_{dry}$ kN/m$^3$ | $\gamma_{sat}$ kN/m$^3$ | *e* | *c* kPa | $\phi$ (degrees) |
|---|---|---|---|---|
| 15.30 | 19.33 | 0.7 | 0 | 44.1 |

Journal of University of Duhok, Vol. 20, No.1 (Pure and Eng. Sciences), Pp 285-292, 2017
eISSN: 2521-4861 & pISSN: 1812-7568
https://doi.org/10.26682/sjuod.2017.20.1.26

Figure 6 shows the normalized ultimat bearing capacity ($\frac{q_{ult}}{s_o}$) versus internal friction angle for different values of parameter $a$: 0.3, 0.5 0.7, 0.9 and 1.2 kPa$^{-1}$. The experimental result represent the ultimate bearing capacity at peal which were plotted at $\phi = 44.1^{o}$. It can be see that the experimental data are reasonably wel defined between the case of $a$ = 0.30 and 0.50 fa away from the initial value of $a$ = 0.7 (red line i Fig. 6). The change of parameter $a$ from 0.7( value of the sand tested to smaller values i possible and it is attributed to the effect of hysteresis of the SWRC (see Fig. 1).

Shwan (2015) observed contraction and dilation phenomena during the application of the load for physical models of a strip footing placed at a surface and direct shear tests. These behaviours were correlated to water migration into or out of the shearing zone (failure mechanisms). This is accompanied by change in void ratio. The implicit of these observations is that the SWRC is shifted to the left hand side due to the change in void ratio leading to a change in $a$ value. Shwan (2016) studied the effect of water migration behaviour in terms of the SWRC for the direct shear tests. Changes of water level in a burette (used to apply and control suction) were observed in the direct shear tests. Samples were taken at the end of the test to further confirm the water migration phenomenon. The analysis showed significant change in the position of the SWRC to the left hand side due to water movement.

The implication of the change in parameter $a$ can be readily seen in Fig. 6 on the bearing capacity due to the hysteresis of the SWRC. The initial shifting of the SWRC at the early stages of the experimental bearing capacity test was accompanied with an increase of degree of saturation and hence a decrease in suction. However; as the footing was further pushed into the soil, drying behaviour beneath and around the footing occurred due to dilation leading to an increase in void ratio. As a subsequent, suction increased which in turns increased bearing capacity.

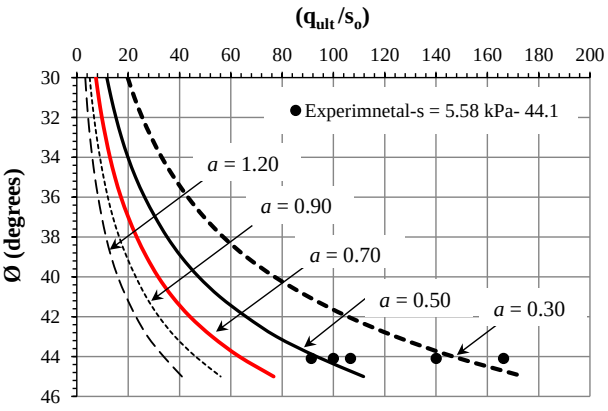


**Fig. (6):** Normalized ($\frac{q_{ult}}{s_o}$) versus $\phi$ for various values of parameter $a$.

Another possible scenario is a change in the air entry value ($s_o$) position on the main drying SWRC during shearing. Different values of $s_o$ are modelled in the modified LimitState:GEO as shown in Fig. 7. The values of ultimate bearing capacity are normalised over unit weight of water ($\gamma_w$) and $H_w$ (= 0.568 m). Cases of $s_o$ between 1 and 3 kPa are close to the experimental results. As stated before, $s_o$ for the used sand is 2.3 kPa which is somewhere in between the experimental data (see red line in Fig. 7), however cannot catch the scatter of the data due to the dilation and hysteresis of the SWRC. It is intriguing, however, that the scenario of changing so is quite possible.

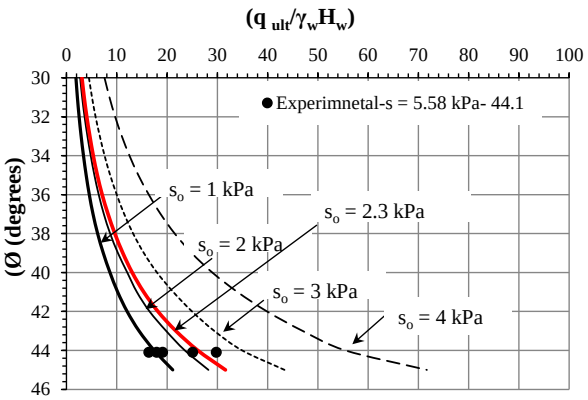


**Fig. (7):** Normalized ($\frac{q_{ult}}{\gamma_w H_w}$) versus $\phi$ for various values of air entry value $s_o$.

Journal of University of Duhok, Vol. 20, No.1 (Pure and Eng. Sciences), Pp 285-292, 2017
eISSN: 2521-4861 & pISSN: 1812-7568
https://doi.org/10.26682/sjuod.2017.20.1.26

**(b) Total Passive Earth Pressure Results**

To investigate further the effect of hysteresis of the SWRC (through parameter $a$ and $s_o$), a retaining wall case study was utlised. A frictional wall ($\phi = \delta$) of 1 m height and 6.2 m in width (x boundary of the problem) with a simulated levelled backfill material (a sandy soil) was modelled in the modified LimitState:GEO software. Two cases of water table position were considered: at the base of the wall ($H_w$ = 0 m) and -0.6 m below the base of the wall (1.6 m from surface of the backfill). These cases are explained in Fig. 8 as cases 1 and 2, respectively. The saturated and dry unit weights of the soil were assumed to be 1.9 and 1.5 of unit weight of water. In the numerical modelling, cohesion $c$ = 0 kPa and a range of internal friction angle values from 30 to 45$^o$ were utilised.

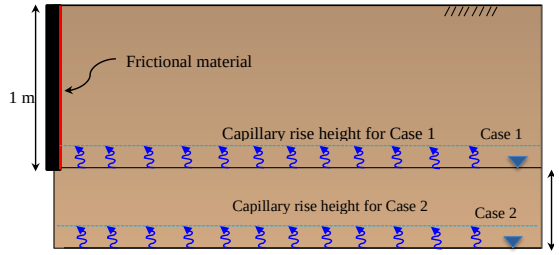


**Fig. (8):** Modelling a retaining wall in the LimitState:GEO software for frictionlal wall.

For each case, different values of parameter $a$: 0.1, 0.2, 0.3 and 0.4 kPa$^{-1}$ (at constant $s_o$) and $s_o$: 3, 4, 5 and 6 kPa (at constant value of $a$) were assumed. This is to investigate the effect of parameter $a$ and $s_o$ independently.

The numerical results for the cases above were compared against the modified Rankine equations which were derived by Shwan (2015) for the total passive pressure. The modified equations take into account the effect of capillary rise for a frictional wall with a levelled backfill.

The modified Rankine equations for cases 1 and 2 are as follows:

1. **For case 1**: $H_w$ = 0 m

$$P_p = \frac{1}{2}k_p \times \gamma_{ave} h_1^2 + [k_p \gamma_{ave} h_1 + (k_p - 1)\gamma_w H_c]H_c + \frac{1}{2}[k_p \gamma_{sat} H_c - (k_p - 1)\gamma_w H_c]H_c + [k_p \gamma_{ave} h_1 + k_p \gamma_{sat} H_c]H_w + \frac{1}{2}[k_p \gamma' H_w^2] + \frac{1}{2}\gamma_w H_w^2 \quad (17)$$

2. **For case 2**: $H_w$ = -0.6 m

$$P_p = \frac{1}{2}k_p \times \gamma_{ave} H^2 \quad (18)$$

where $\gamma_{ave}$, $\gamma_{sat}$ and $\gamma'$ are average, saturated and buoyant unit weights, respectively. $H_c$ is capillary rise height (given by Eq. 9), $H_w$ is distance from the wall base to water table (positive upwards) and $H$ is height of the wall. $h_1$ is distance from capillary rise to surface ($h_1 = H - H_w - H_c$) and $k_p$ is passive earth pressure coefficient. Values of $k_p$ at different internal friction angle for a frictional wall is based on Eurocode 7 (2004) as shown in Fig. 9.

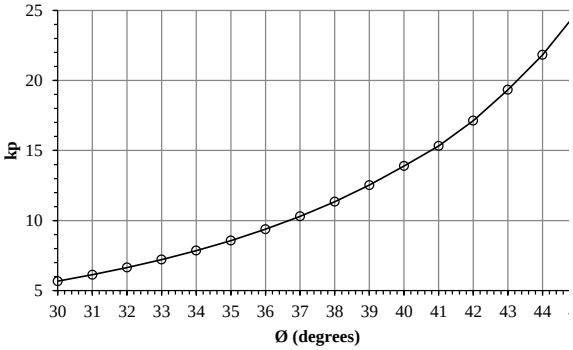


**Fig. (9):** Values of $k_p$ for a frictional wall for a range of $\phi$ values, after Eurocode 7 (2004).

Figure 10 represents the results of case 1 ($H_w$ = 0 m for different values of parameter $a$ at constant initial value of $s_o$ = 5 kPa (obtained from the SWRC of the work of Krishnapillai and Ravichandran (2012)). Higher values of parameter $a$ provide smaller normalized total passive earth pressure. This is attributed to the effect of hysteresis of the SWRC during shearing which causes shifting of the SWRC to the left hand side. The normalized $P_p$ decreased by a factor of 1.08 when the SWRC shifted from $a$ = 0.1 to 0.4 at $\phi = 30^o$.

Figure 11 shows the effect of $s_o$ at constant $a$ = 0.1 kPa$^{-1}$ for $H_w$ = 0 m. Smaller values of $s_o$ than the initial $s_o$ = 5 kPa is more reasonable than the case $s_o$ = 6 kPa. This due to the fact that shifting of the SWRC to right hand side is not possible. Inspection from Figs. 10 and 11 suggests that case when $a$ is changing during shearing is more likely to occur than change of $s_o$.

Journal of University of Duhok, Vol. 20, No.1 (Pure and Eng. Sciences), Pp 285-292, 2017
eISSN: 2521-4861 & pISSN: 1812-7568
https://doi.org/10.26682/sjuod.2017.20.1.26

Figures 12 and 13 reveal the numerical results for case 2 ($H_w$ = -0.6 m). The difference between the numerical results and the Rankine method is bigger at higher $\phi$ values. This is because the contribution of capillary rise on the Rankine Equation (Eq. 18) is negligible as the water table is below the base of the wall.

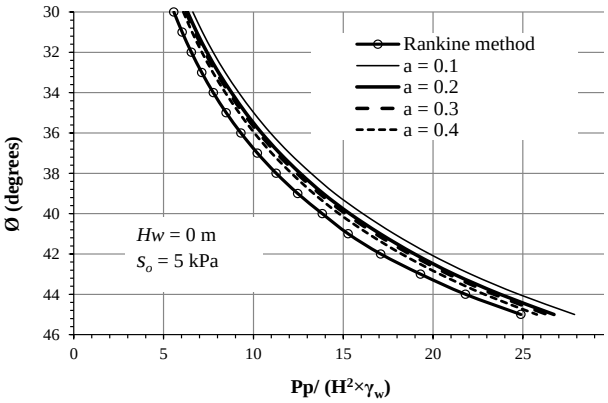


**Fig. (10):** Normalized ($\frac{P_p}{H^2 \times \gamma_w}$) versus internal friction angle for different values of $a$ at $s_o$ = 5 kPa and $H_w$ = 0 m.

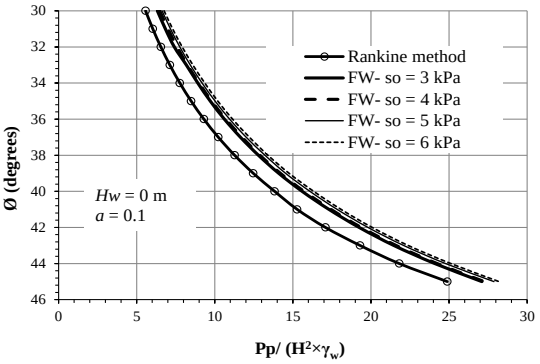


**Fig. (11):** Normalized ($\frac{P_p}{H^2 \times \gamma_w}$) versus internal friction angle for different values of $s_o$ at a = 0.1 kPa$^{-1}$ and $H_w$ = 0 m.

A comparison between Figs. 10 and 12 clearly shows that the effect of $a$ for the case when $H_w$ is below the wall base is higher due to the higher applied suction. Once again, the possibility of changing parameter $a$ is more noticeable as shown in Figs. 12 and 13.

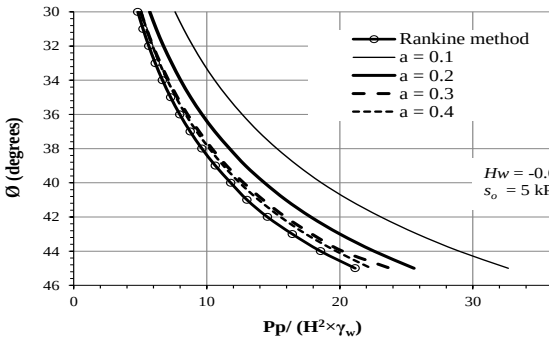


**Fig. (12):** Normalized ($\frac{P_p}{H^2 \times \gamma_w}$) versus internal friction angle for different values of $a$ at $s_o$ = 5 kPa and $H_w$ = -0.6 m.

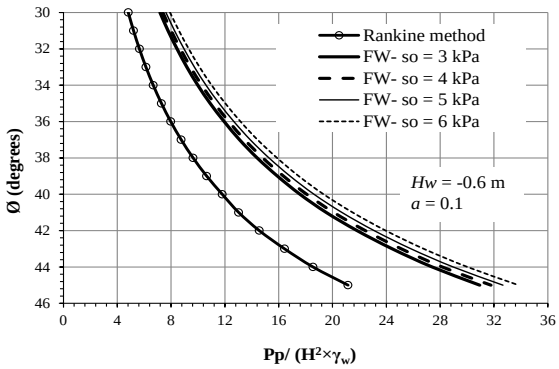


**Fig. (13):** Normalized ($\frac{P_p}{H^2 \times \gamma_w}$) versus internal friction angle for different values of $s_o$ at $a$ = 0.1 kPa$^{-1}$ and $H_w$ = -0.6 m.

## 7. CONCLUSIONS

This paper presents a modification of an existing soil water retention curve (SWRC) equation. The modification of the SWRC equation took into account the effect of the soil capillarity (parameter $a$) and air entry value ($s_o$). The modified SWRC equation was then incorporated into a research version of the LimitState:GEO software where the effects of suction and degree of saturation on strength were taken into consideration. The modified LimitState:GEO then utilised to perform parametric studies of bearing capacity and total

passive earth pressure where the effect of SWRC hysteresis was considered.

The numerical results for different values of *a* and $s_o$ showed reasonable agreement with the experimental peak bearing capacity and total passive earth pressure data. The latter was validated against the modified Rankine earth pressure equations. The scattering due to the effect of dilation and compression for the experimental bearing capacity data was reasonably well defined among different values of parameter *a* or $s_o$ due to the hysteresis of the SWRC.

## REFERENCES


- Brooks, R. H. & Corey, A. T. 1964. Hydrulic properties of porous medium *Colorado State University (Fort Collins), Hydrology Paper*.
- Fredlund, D. G. & Rahardjo (eds.) 1993. *Soil* Mechanics *for unsaturated soils*.
- Fredlund, D. G. & Xing, A. 1994. Equation for soil-water characteristic curve. *Canadian Geotechnical Journal,* 31**,** 521-532.
- Krishnapillai, S. H. & Ravichandran, N. 2012. New soil-water characteristic curve and Its performance in the finite-element simulation of unsaturated soils. *International J. of Geomechanics,* 12**,** 209-219.
- Öberg , A. L. & Sällfors, G. 1997. Determination of shear strength parameters of unsaturated silts and sands based on the water retention curve. *Geotechnical testing,* 20**,** 40-48.
- Shwan, B. 2016. Moisture migration during loading and shearing of unsaturated sand. *3rd European Conference on Unsaturated Soils - "E-UNSAT 2016".* Paris, France.
- Shwan, B. J. 2015. *Experimental and Numerical Study of the Shear Strength of Unsaturated Sand.* PhD Thesis, The University of Sheffield.
- Shwan, B. J. & Smith, C. C. 2014. Application of limit analysis in unsaturated soils: numerical and experimental study of bearing capacity. *In Unsaturated Soils: Research and Applications - Proceedings of the 6th International Conference on Unsaturated Soils, UNSAT 2014* Sydney, Australia.
- Standard, B. 2004. Eurocode 7: Geotechnical design.
- Stanier, A. A. & Tarantino, A. 2010. Active earth force in 'cohesionless' unsaturated soils using bound theorems of plasticity. *In: Alonso, E.E., Gens, A. (Eds.), Proceedings of 5th International Conference on Unsaturated Soils, CRC Press, Barcelona, Spain.*
- Van Genuchten, M. T. 1980. A closed-form equation for predicting the hydraulic conductivity of unsaturated soils. *Soil Science Society of America Journal,* 44**,** 892-898.
- Vanapalli, S., Fredlund, D., Pufahl, D. & Clifton, A. 1996. Model for the prediction of shear strength with respect to soil suction. *Canadian Geotechnical Journal,* 33**,** 379-392.